Journal of Materials Chemistry B

ROYAL SOCIETY OF CHEMISTRY

PAPER

View Article Online
View Journal | View Issue

Cite this: J. Mater. Chem. B, 2024, 12, 4409

Tetramethylpyrazine-loaded electroconductive hydrogels promote tissue repair after spinal cord injury by protecting the blood–spinal cord barrier and neurons†

Bowen Deng,‡[ab] Shengyuan Jiang,‡[b] Gang Liu,‡[b] Xiaoye Li,[b] Yi Zhao,[b] Xiao Fan,[d] Jingpei Ren,[b] Chengyun Ning,[c] Lin Xu,[b] Linhong Ji*[a] and Xiaohong Mu*[b]

Spinal cord injury (SCI) usually induces profound microvascular dysfunction. It disrupts the integrity of the blood–spinal cord barrier (BSCB), which could trigger a cascade of secondary pathological events that manifest as neuronal apoptosis and axonal demyelination. These events can further lead to irreversible neurological impairments. Thus, reducing the permeability of the BSCB and maintaining its substructural integrity are essential to promote neuronal survival following SCI. Tetramethylpyrazine (TMP) has emerged as a potential protective agent for treating the BSCB after SCI. However, its therapeutic potential is hindered by challenges in the administration route and suboptimal bioavailability, leading to attenuated clinical outcomes. To address this challenge, traditional Chinese medicine, TMP, was used in this study to construct a drug-loaded electroconductive hydrogel for synergistic treatment of SCI. A conductive hydrogel combined with TMP demonstrates good electrical and mechanical properties as well as superior biocompatibility. Furthermore, it also facilitates sustained local release of TMP at the implantation site. Furthermore, the TMP-loaded electroconductive hydrogel could suppress oxidative stress responses, thereby diminishing endothelial cell apoptosis and the breakdown of tight junction proteins. This concerted action repairs BSCB integrity. Concurrently, myelin-associated axons and neurons are protected against death, which meaningfully restore neurological functions post spinal cord injury. Hence, these findings indicate that combining the electroconductive hydrogel with TMP presents a promising avenue for potentiating drug efficacy and synergistic repair following SCI.

Received 16th September 2023,
Accepted 6th April 2024

DOI: 10.1039/d3tb02160b

rsc.li/materials-b

1. Introduction

Spinal cord injury (SCI) is a highly disabling neurological disease, with no effective treatment strategies for neurological repair yet. Neuronal loss and axon and myelin necrosis at the injury site and the interface between normal tissues and lesions post-trauma are critical factors limiting the effectiveness of SCI treatment.[1] Unfortunately, the death of neuron-endothelial cells at the core of the injury site is inevitable after SCI. However, strategizing to mitigate programmed cell death at the adjacent interfaces of lesions and foster the migration and differentiation of reserve cells towards the epicenter for remodeling the neurovascular unit holds promise as a potential approach for neural restoration.[1,2] Traumatic spinal cord injury is immediately followed by disruption of the microvascular structure, mainly with the breakdown of the blood–spinal cord barrier (BSCB). Increased BSCB permeability leads to extravasation of hematogenous substances at the injury nexus, which manifests as perivascular parenchymal changes and vasogenic edema; furthermore, it also progressively extends along the spinal axis, exacerbating damage in the adjacent regions.[3] These exudates trigger a cascade of complex pathological processes including neurotoxic product generation, oxidative stress response, and inflammatory cell infiltration, resulting in

[a] Division of Intelligent and Biomechanical System, State Key Laboratory of Tribology, Department of Mechanical Engineering, Tsinghua University, Beijing, 100084, China. E-mail: jilh@tsinghua.edu.cn
[b] Department of Orthopedics, Dongzhimen Hospital, Beijing University of Chinese Medicine, Beijing, 100700, China. E-mail: muxiaohong2006@126.com
[c] College of Materials Science and Technology, South China University of Technology, Guangzhou 510641, Guangdong Province, China
[d] Department of Orthopedics, Qingdao Municipal Hospital, Qingdao, 266071, Shandong Province, China

† Electronic supplementary information (ESI) available: Table S1: the thickness of the skin's inflammatory layer. Tables S2 and S3: the results of BBB score and the inclined plate test. Fig. S1: physical properties of hydrogels. Fig. S2 and S3: biocompatibility of the hydrogels. Fig. S4: degradation properties of various implanted hydrogels. Fig. S5: HE and Masson staining results of spinal cord tissues at 28 days post-injury. Fig. S6: alteration of neurofilaments (NF) in the injury site. See DOI: https://doi.org/10.1039/d3tb02160b

‡ These authors contributed equally to this work.

the programmed death of neurons at lesions and interface of the injury site that may even lead to permanent neurological deficits.[3,4] Notably, the loss of BSCB integrity is detrimental to the maintenance of homeostasis of the internal environment of the spinal cord, and it also impacts the generation of blood vessels that act as a scaffold for axonal regeneration.[5,6] Thus, it is significant to target BSCB repair at an early stage of SCI to mitigate peri-lesional cellular perturbations and thereby modulate neuronal network homeostasis.[3,7,8] Furthermore, it may provide a foundation for neuronal repair and myelinated axon growth.

The therapeutic goal of BSCB repair is to preserve the survival and structural integrity of critical cells in their substructures.[3] Several studies have confirmed that protecting the endothelial cell integrity and reducing the decreased expression level of tight junction proteins (ZO-1 and occuldin) is effective in maintaining the normal BSCB to mitigate secondary injury and is also an important therapeutic target for drugs or novel molecules.[3,9,10] Plant-derived bioactive compounds such as tetramethylpyrazine (TMP), tanshinone IIA, and curcumin have demonstrated potential in BSCB repair.[11] TMP is extracted from the rhizome of the Traditional Chinese herb *Ligusticum chuanxiong* and constitutes a small molecule of the herb. Notably, TMP has significant vascular protective effects.[12] The latest meta-analysis indicated that injecting TMP as an adjunctive treatment seemed effective in enhancing the efficacy of acute cerebral infarction and improvement in neurological deficit scores of patients.[13] Meanwhile, diverse pharmacological activities of TMP in protecting barrier integrity have also been validated. TMP may exert neuroprotective effects by regulating multiple signaling pathways to promote tight junction protein expression and inhibiting extracellular matrix degradation by matrix metalloproteinases-9, thereby reducing barrier permeability.[14–17] It also considerably protects the tight junction proteins of the endothelial cells to alleviate the disruption of the BSCB by modulating microglia polarization from a M1 phenotype to a M2 phenotype through inhibition of NF-κB pathways.[15] Moreover, TMP can attenuate oxidative stress and anti-apoptosis to protect against endothelial injury.[18,19] TMP is a naturally derived product that is a potential therapeutic agent in the treatment of SCI due to its efficacy and affordability; however, its application is limited by its short half-life and poor bioavailability.[20]

Recently, conductive biomaterial scaffolds have emerged as an innovative therapeutic strategy to promote neuronal regeneration, angiogenesis, and BSCB repair following SCI by equipping exogenous regulatory factors and/or seed cells, which consequently promotes the recovery of neurological functions.[21–25] In particular, electroconductive hydrogels with a unique three-dimensional mesh structure and a hydration form are similar to natural nerve tissues with respect to the design and elastic modulus, which facilitates cell adhesion and drug delivery. Its ability to mimic the electrical transmission properties of native nerve tissues provides electrical cues for cell regeneration and enhances SCI repair. Simultaneously, it can effectively respond to external electrical stimulation and synergistically induce neural stem cells to differentiate into neurons.[22,26–28] Previous studies have indicated that conductive polymer hydrogels constructed with the addition of polypyrrole materials may effectively stimulate the recruitment of endogenous neural stem cells and accelerate neurological recovery after SCI.[22,23,26] Moreover, using electroconductive hydrogels as scaffolds for mesenchymal stem cell-derived exosomes achieves dual objectives of enhancing exosome stability and facilitating drug encapsulation accompanied by sustained release.[22] Furthermore, it also synergistically enhances neural restoration. Therefore, integrating therapeutical medicine within conductive hydrogels is a potentially ground breaking therapeutic strategy that is poised to substantially enhance functional recovery after SCI, while optimizing the spatial distribution and bioavailability of drugs within lesions.

In view of this, based on our previous studies, we developed innovative conductive hydrogels loaded with TMP, which synergistically exert therapeutic effects of repairing the BSCB and protecting neurons and axons, while enhancing the bioavailability of the drug. To actualize this multifunctional hydrogel paradigm, we ingeniously incorporated TMP into a matrix of methacrylic gelatin (GM) and polypyrrole (PPy). Using photocrosslinking, we subsequently constructed conductive hydrogels that demonstrated properties such as softness and hydration. Owing to the conjugated double bonds that are inherent in TMP, an interaction occurs with the conjugated double bonds in PPy, resulting in a pronounced π–π stacking effect. However, this reversible interaction remains benign for the structural integrity and bioactivity of TMP, which enhances the therapeutic stability as well as ensures a gradual and sustained release of the compound in the initial phases after implantation. Furthermore, we assessed the biocompatibility of the tetramethylpyrazine-loaded electroconductive hydrogel (GMPT) with experiments both *in vitro* and *vivo*. We used a rat model with complete spinal cord transection and scrutinized the efficacy of GMPT implantation in enhancing the neurological functional recovery. We further identified associated signaling pathways involved in BSCB repair *via* GMPT.

2. Materials and methods

2.1. Synthesis of GM-PPy (GMP) and GMPT hydrogels

A GM monomer was synthesized as described previously.[22,29] In brief, 0.5 mL of methacrylic anhydride was added to the 10% (w/v) gelatin solution and incubated for 1 h. After dialysis of the mixed solution through deionized water, the GM monomer was further lyophilized for future use. GM hydrogels were synthesized by UV cross-linking of a 3% (w/v) GM monomer and a 0.5% photoinitiator. PPy was synthesized by mixing solution A containing 70 μL of pyrrole (Py) with solution B containing 0.316 mg of ferric chloride hexahydrate at 4 °C. Then, the 3% (w/v) GM monomer, 0.5% photoinitiator (Irgacure 2959; Sigma), and 0.03 g PPy were dissolved in 1 mL of deionized water at 60 °C to obtain solution C. The GM-PPy (GMP) hydrogels were prepared by UV cross-linking (6.9 mW cm^{-2},

360–480 nm) of solution C under light-protected conditions and immersed into PBS buffer at 4 °C overnight to clear any uncross-linked products. GMPT hydrogels were prepared as follows: the TMP dose was determined by our preliminary experiments and literature reports.[30] 30 mg of TMP was dissolved in 1 mL of deionized water to obtain a solution, and it was then added into solution C to obtain a mixed solution. Finally, the GMPT hydrogel was prepared by UV cross-linking of this solution.

2.2. Characterization of hydrogels

2.2.1. Morphology and composition properties of hydrogels. Hydrogel samples were prepared by freeze-drying under vacuum prior to the experiment. Samples were flash frozen for 20 s using liquid nitrogen before sputter coating with platinum (Pt) for 60 s. A SEM (Nova Nano, FEI) was used to observe the microscopic morphology at an accelerating voltage of 10.0 kV. A Fourier-transform infrared (FTIR) spectrometer (Nicolet6700, Thermo Fisher) was used to obtain the spectra of GMP and GMPT hydrogels. The samples were freeze-dried before being ground with potassium bromide powder and pressed into tablets. Thereafter, the spectra of samples were detected in the range of 400–4000 cm^{-1}.

2.2.2. Drug release of hydrogels *in vitro*. The GMPT hydrogel (1 g) was incubated in 50 mL of PBS buffer (pH 7.4, 37 °C), and the supernatant was collected every 24 hours. The concentration of TMP released in the supernatant was established by ultraviolet-visible absorption spectroscopy. Before calculating the drug release rate based on the TMP concentration of the supernatant, the absorbance of the drug was measured and compared with the calibration curve to validate the linear relationship between the drug content and the absorbance.

2.2.3. Rheological properties of hydrogels. The rheological properties of hydrogel samples were tested using a rotary rheometer (Physica MCR301, Anton Paar). The sample was placed on the lower plate of the equipment and preheated to 37 °C before the measurement. The upper plate of the machine was slowly lowered to the top of the sample, and the sample was frequency swept at a fixed strain of 1%. Finally, the average storage modulus was calculated separately for each group at 1 Hz and the statistical analysis was performed.

2.2.4. Electrical properties of hydrogels. The electrical characterization methods of hydrogel samples, including CV and EIS, were performed using an electrochemical workstation (ZAHNER, Zennium, Germany). The hydrogel-coated indium tin oxide (ITO) glass was used as the working electrode, while platinum mesh and silver/silver chloride were used as the counter and reference electrodes. For CV measurements, the samples were performed at a scan rate of 10 mV s^{-1}, ranging from −0.2 to 0.4 V in PBS solution. The samples were measured by EIS within the open circuit potential range of 100 kHz to 0.01 Hz, using a compensation amplitude of 5 mV.

2.2.5. Biocompatibility of hydrogels *in vitro*. Neural stem cells (NSCs) were used for the evaluation of the *in vitro* biocompatibility of each hydrogel. The C17.2 neural stem cells were purchased from PriCells and cultured in a high glucose DMEM (PM150210, Procell) containing 10% fetal bovine serum (SH30084.03, HyClone). The third to fifth-generation cultured cells were used for subsequent experimental studies. The C17.2 cells were harvested and counted during their logarithmic growth phase. The resuspended cells with a density of 2×10^5 cells per well were incubated with the medium in a 6-well tissue culture plate for 24 h at 37 °C, before the cell adhesion to the plate was evaluated. Subsequently, the GM, GMP, and GMPT hydrogels were completely immersed in the responding medium with a concentration of 45 mg mL^{-1} for 24 h. The hydrogel extract was then incubated with 6-well plate seed cells for another 24 h. The cellular proliferation on hydrogels was evaluated using the CCK-8 assay (C0037, Beyotime, China) at days 1, 3 and 7 of co-culture. After removing the culture medium, the cells were washed 3 times with PBS and then replaced with a medium solution containing 10% v/v CCK-8 to incubate in a dark room for 4 h. The 100 μL supernatant mixture solution was transferred to a 96-well tissue culture plate and measured with a microplate reader at the 450 nm wavelength. The viability of NSCs on hydrogels was evaluated using calcein-AM/PI (C2015S, Beyotime, China). As previously described,[22,29] after the medium was removed, calcein-AM and PI were added to the culture medium and double-stained in 5% CO_2 at 37 °C for 30 min. After washing three times with PBS, images capturing the live/dead cellular distinction were obtained using a microscope.

2.2.6. Degradation and biocompatibility of the hydrogels *in vivo*. We implanted hydrogels in the back and spinal cord of female Sprague–Dawley rats to evaluate the *in vivo* biodegradability and biocompatibility of each hydrogel.

(i) Hydrogel degradability: the GM, GMP, and GMPT hydrogels were prepared in standardized cylindrical shapes (8 mm × 2 mm) and subcutaneously implanted in the back of the rats and removed at days 7, 28, and 56 after the operation. The surrounding tissue was collected to observe hydrogel degradability compared with normal tissues. The pathological condition of skin inflammation was further analyzed using HE staining.

(ii) Hemocompatibility: the arterial blood samples of female SD rats (180 ± 20 g, $n = 6$) were collected in sodium heparin tubes. Equal-quality GM, GMP, and GMPT hydrogels were added to the tubes for experimentation. Saline and deionized water were added to the heparin tubes for negative and positive controls. After the samples were incubated inside the incubation box at 37 °C for 4 h, the supernatant was extracted by high-speed centrifugation for 5 minutes at 12 000 rpm and 4 °C. The absorbance of each group of supernatants was measured at 545 nm using a microplate reader (Molecular Devices, USA) to determine the hemolysis rate (HR) of each group.

$$\mathrm{HR}\ (\%) = \frac{\text{experimental absorbance} - \text{negative control}}{\text{positive absorbance} - \text{negative control}} \times 100 \quad (1)$$

(iii) Tissue compatibility: female SD rats (240 ± 10 g, $n = 18$) were divided into sham, SCI, and GMPT groups according to

the random number table by investigators. The complete transaction animal model was constructed. Rats were then sacrificed at 28 days post-injury to obtain arterial blood samples and tissues. The erythrocyte sedimentation rate (ESR) and C-reactive protein (CPR) in serum samples were analyzed using a hemorheometer and the ELISA assay (SEKR-0017, Solebro). The internal organs of the rats *i.e.*, heart, liver, spleen, lungs, kidneys, and small intestine were collected for hematoxylin and eosin (H&E) staining to observe inflammatory infiltrates around the lesions. In addition, after immunohistochemical staining of the spinal cord tissue at the injury site, the expression of inflammatory markers (NF-κB, TNF-α, and IL-10) was semi-quantitatively analyzed using the Image J software.

2.3. *In vivo* studies

2.3.1. Ethics statement. Experiments were performed under a project license (NO. BUCM 2021040802-2029) granted by the Committee on the Ethics of Animals of Beijing University of Chinese Medicine and complied with institutional guidelines for the care and use of animals.

2.3.2. Experimental groups and spinal cord injury model. Female SD rats (240 ± 10 g, n = 150) were randomly divided into five equal groups as follows: (a) sham group (T9-T10 laminectomy + saline), (b) SCI group (SCI + saline), (c) TMP group (SCI + TMP), (d) GMP group (SCI + GMP implantation + saline), and (e) GMPT group (SCI + GMPT implantation + saline). The drug dose in the TMP group was 25 mg kg^{-1} (Harbin Sanlian Pharmaceutical Co., Ltd), as determined by the dose conversion factor for humans and rats and literature reports.[31] The rats in the sham, SCI, GMP, and GMPT groups were injected with an equal volume of saline. All SD rats were injected intraperitoneally once daily for 7 days with the above designed formulations as TMP or saline.

The spinal cord was completely transected at the level of T9–T10 in the rats. Before the surgery, the animals were anesthetized by an intraperitoneal injection of ketamine–xylazine (75 mg kg^{-1} ketamine, 5 mg kg^{-1} xylazine). Next, the surgery was performed to prepare a complete transection model by removing the spinal cord tissue at the T9–T10 level, leaving a 2 mm gap. In brief, the vertebral plates of rats were removed at the 9th and 10th thoracic vertebra levels to reveal the thoracic 9th spinal cord level. Then, it was completely transected by self-made double-edged microsurgical scissors, and we observed whether the ventral spinal cord was resected entirely under a microscope. The gelatin sponge was subsequently placed between the muscle layer and the vertebral plate to prevent the secondary effects of the muscle layer on the lesions, followed by three-layer suturing to close the longitudinal incision. In the sham group, only the thoracic spine plate was removed and then closed. The rat bladder was emptied manually twice daily until spontaneous voiding resumed.

2.3.3. Behavior tests. The recovery of the hindlimb motor function for rats was assessed at pre-operative and five observational time points after injury (1 d, 3 d, 7 d, 14 d, and 28 d) using the Basso, Beattie, and Bresnahan (BBB) score and the modified Rivlin–Tator angleboard test.[32] Two investigators performed a BBB rating scale score to evaluate the hindlimb motor score of injured animals in an open field (1 m side length). The inclined plate test aimed to better estimate the motor function and limb coordination of the hind limbs of rats with injury. The function recovery of animals was analyzed by observing the maximum tilt angle in maintaining the limb balance on the plate for 5 seconds.

2.3.4. Histological analysis. Animals were sacrificed, and samples were taken at days 7 and 28 after injury. Meantime, the skin tissues were taken at days 7, 14 and 56. Partial rats were perfused with 0.9% NaCl and fixed with 4% paraformaldehyde. The spinal cord with the lesions and internal organs was removed, embedded in paraffin and cut into 5 μm sections for staining. The part of spinal cord samples for rats were collected for fresh frozen and embedded with the Tissue-Tek® OCT compound (Sakura, California) at −20 °C. 15 μm thick longitudinal slices were obtained using standard techniques for future use. HE staining was used to observe inflammatory infiltrates in internal organs, skin tissues, and the distance between the broken ends of the spinal cord gap. Masson staining was performed to evaluate collagenous tissue deposition, which was analyzed using Image J to calculate the collagen volume fraction. To reveal Nissl bodies and demyelination, sections were stained with Nissl and LFB according to the standard procedures.

2.3.5. ELISA assay. Enzyme-linked immunosorbent assay (ELISA) kits were used to investigate the expression levels of SOD, MDA, GSH, and ROS (MLBio, Shanghai, China) for the fresh frozen spinal cord tissue according to the manufacturer's instructions at 7 days and 28 days after the damage. The absorbance was detected at 450 nm using a microplate reader (EMAX Plus, USA); thereafter, the concentrations of SOD, MDA, GSH, and ROS were calculated from standard curves.

2.3.6. Immunohistochemical staining. The paraffin-embedded spinal cord tissue was cut into a 5 μm section on the 7th and 28th days after the injury for immunohistochemistry (IHC) analysis. Paraffin pieces were dewaxed, rehydrated, and then used in citrate buffer (pH 6.0) for antigen retrieval. The slides were blocked with 3% hydrogen peroxide for 30 min at room temperature before blocking with 3% BSA for 30 min at 37 °C. Samples were further incubated with NF-κB (1 : 100, 66535-1-Ig, Proteintech), TNF-α (1 : 200, ab220210, Abcam), IL-10 (1 : 50, 60269-1-Ig, Proteintech), ZO-1 (1 : 200, ab221547, Abcam), and occludin (1 : 50, 66378-1-Ig, Proteintech) overnight at 4 °C. Then, the slices were flushed and incubated with the secondary antibody for 30 min, followed by DAB for color development. Finally, the samples were counterstained with hematoxylin for 5 min and dehydrated by ethanol before sealing with coverslips.

2.3.7. Immunofluorescent staining. The frozen spinal cord slices were thawed at 37 °C and pre-incubated with PBS containing 0.2% Triton-100X for 10 min at room temperature. The sections were then blocked with 10% FBS (SH30084.03, HyClone) for 1 h and incubated overnight with CD31 (1 : 2000, Ab76533, Abcam), caspase3 (1 : 100, 66470-2-Ig, Proteintech), and NF200 (1 : 200, 18934-1-AP, Proteintech) at 4 °C. The corresponding second antibody was then added to the sections

and incubated for 1 h. The nuclei were stained with DAPI (ab104139, Abcam) before imaging.

2.3.8. Western blotting. On weeks 1 and 4 after the injury, the spinal cord tissues in lesions were dissolved to extract total proteins with RIPA lysis buffer (Solarbio, China). After determining the protein concentration using a BCA assay kit (Thermo, USA), the proteins were detached using 10% sodium dodecyl sulfate–polyacrylamide gel electrophoresis (PAGE). Thereafter, the proteins were transferred to polyvinylidene fluoride (PVDF) membranes, which were blocked with 0.1% TBS-T containing 5% skim milk powder for 1 h. Subsequently, primary antibodies were added to the membranes at 4 °C including PI3K (1 : 2000, 60225-1-Ig, Proteintech), p-PI3K (1 : 1000, ab182651, Abcam), AKT (1 : 3000, 10176-2-AP, Proteintech), p-AKT (1 : 1000, 66444-1-Ig, Proteintech), Bax (1 : 1000, 60267-1-Ig, Proteintech), Bcl-2 (1 : 1000, 26593-1-AP, Proteintech), and caspase3 (1 : 500, 19677-1-AP, Proteintech) and kept overnight. After washing with TBS-T, the membranes were incubated with corresponding secondary antibodies for another 1 h. Finally, protein bands were visualized with an enhanced chemiluminescence (ECL) developer and analyzed using the Image J software.

2.4. Statistical analysis

The SPSS 27.0 software (IBM, USA) was used to analyze the data. Results of data with the normal distribution were expressed as mean ± standard deviation (mean ± SD). One-way ANOVA was used for multiple group comparisons with equal variances, and non-parametric tests were used if the data failed to demonstrate equal variances. The measures that did not conform to the normal distribution were expressed as a median with the interquartile range. Independent *t*-tests and rank-sum tests were used for comparison between groups.

3. Results

3.1. Fabrication and mechanical properties of hydrogels

We fabricated GMPT hydrogels by employing a sequential synthesis approach, building upon established methodologies from previous research studies. Initially, the GM hydrogel network was formed by UV cross-linking. Subsequently, the GM hydrogel was sequentially immersed in a solution containing the Py monomer to construct an opaque GMP hydrogel, which exhibited the characteristic peaks of GM and PPy in the FTIR spectrum (Fig. 1G). The characteristic absorption band for GM at 1650 cm^{-1} was due to the stretching of the C═O bond (amide I). PPy exhibited the characteristic band of Py ring vibration at 1542 cm^{-1}, while the band at 1035 cm^{-1} was ascribed to C–H in-plane deformation. The peak at 902 cm^{-1} could be attributed to the stretching vibrations of the C═N + –C bonds. TMP was then loaded into the GMP hydrogel network, leveraging the conjugated double bonds present in both TMP and PPy that manifested as π–π stacking interactions. Scanning electron microscopy (SEM) analyses showed that the GM hydrogel had optimal porosity, while the combination of PPy and TMP did not disrupt the three-dimensional porous network structure of the GM hydrogel. Consequently, the GMPT hydrogel also manifested a three-dimensional porous structure (Fig. 1C). This intricate structure was conducive to cellular adhesion and growth and offered an optimal microenvironment for the regeneration of axons and the microvasculature. The rheological evaluation demonstrated that the storage modulus (elastic modulus, G') consistently exceeded the loss modulus (viscous modulus, G'') within the angular frequency range of 0.1–10 Hz for all the hydrogels. The combination of PPy and TMP elevated the storage modulus of the hydrogels to varying degrees, thereby enhancing their mechanical strength. At a frequency of 1 Hz, the average storage moduli of GM, GMP, and GMPT hydrogels increased progressively at 656 ± 106.86 Pa, 1300 ± 62.4 Pa, and 1473.33 ± 55.08 Pa, respectively. Notably, the average storage moduli of GMP and GMPT hydrogels exhibited statistically significant differences compared to that of the GM hydrogel ($P < 0.001$). Furthermore, these values were matched with the mechanical properties of neural tissues, which ranged from 600 to 3000 Pa (Fig. 1E and F). In addition, the GMPT hydrogel had excellent adhesion properties and could effectively adhere to the isolated spinal cord for better therapeutic results for nerve repair (Fig. 1D).

Cyclic voltammetry (CV) and electrochemical impedance spectroscopy (EIS) tests were performed to investigate the electrochemical properties of the hydrogels. The GM hydrogel group showed negligible response currents in voltage scanning, whereas GMP and GMPT hydrogels showed improved anodic and cathodic currents (Fig. S1A and B, ESI†). The CV curves indicated that both the conductive hydrogels exhibited comparable oxidation and reduction current values. The EIS image revealed that the Nyquist plot of the GMP and GMPT hydrogels in the high-frequency region exhibited a similar quasi-semicircle, indicating good redox activity in both hydrogels. The radius of the circle of the GMPT hydrogel was slightly increased compared to that of the GMP hydrogel; however, the difference was minimal, suggesting lower charge transfer resistance (Fig. S1A, ESI†). The results from the EIS analysis were according to the CV data, indicating that the combination of PPy enhanced the electroactivity of the hydrogel. Notably, TMP loading did not affect the electrochemical properties of the hydrogel. Moreover, employing the four-probe method to obtain the electrical resistivity data of the three hydrogels revealed the GMP and GMPT hydrogel values as 1.83×10^{-3} and 1.49×10^{-3} S cm^{-1}, respectively, with no significant difference between them (Fig. S1C, ESI†). The data demonstrated that the electrical properties of the GMP and GMPT hydrogels were similar. Therefore, the combination of TMP had no considerable influence on the electrical properties of the conductive hydrogels.

The drug delivery capability of GMPT hydrogels was evaluated further. Utilizing a microplate reader, we characterized the absorption curve of the TMP standard. The spectral analysis revealed a prominent absorption peak at 295 nm for TMP. The linear regression equation was determined as $Y = 0.0132 + 0.032X$ with a correlation coefficient (R) of 0.9994, indicating a

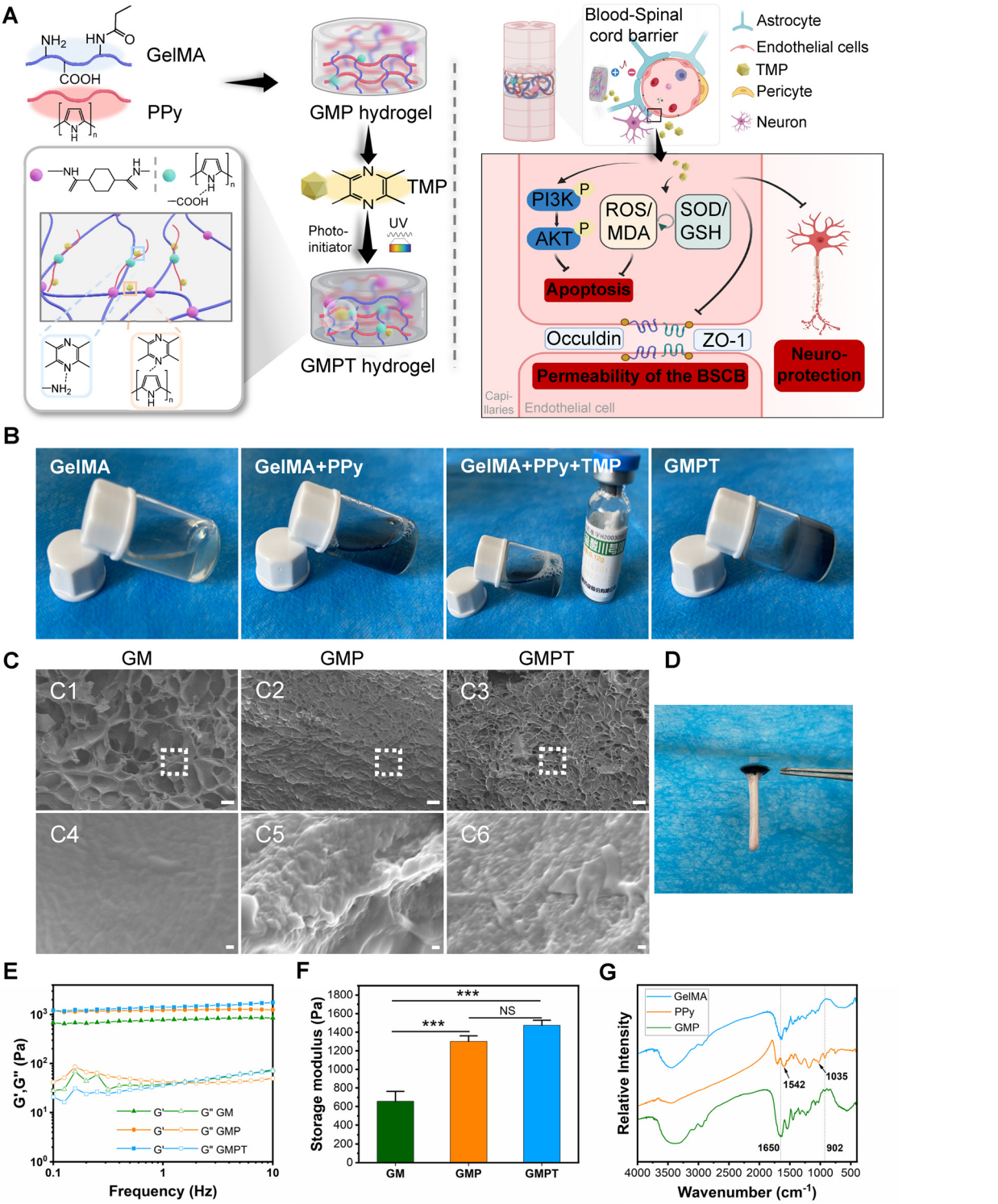

Fig. 1 Characteristics of different hydrogels. (A) Schematic representation of hydrogel synthesis and its potential mechanism in the treatment of spinal cord injuries. (B) Photographs showing polymerization occurring with different combinations of reagents. (C) The microstructures of GM, GMP, and GMPE hydrogels as observed by SEM images (C1–C3) and higher magnification SEM images (C4–6). The scale bars are 30 μm and 200 nm. (D) GMPT hydrogel effectively adhered to freshly harvested spinal cords from the rats. The mechanical properties of different hydrogels were evaluated by rheological analysis. The images showed the variation curves of the storage and loss moduli of GM, GMP, and GMPE hydrogels (E) and the storage modulus of the three groups of hydrogels at 1 Hz (F). (G) FTIR spectroscopy analysis was used to identify functional groups in the synthesized hydrogel. Groups were analyzed with a one-way ANOVA and a Bonferroni multiple comparison test (***$P < 0.001$).

robust linear relationship within the concentration range of 0–50 μg mL^{-1} (Fig. S1D and E, ESI†). Based on established standard parameters, the cumulative release of TMP from the GMPT hydrogel at various time points was quantified, as illustrated in Fig. S1F (ESI†). Meanwhile, TMP could be sustained in GMPT hydrogels, with an accumulative release of 80.3% by day 14. Thus, it could be inferred that TMP was effectively loaded into the GMPT hydrogel, facilitating its prolonged and sustained release.

3.2. Biocompatibility and degradability of the hydrogels

Good biocompatibility and appropriate degradability are essential properties for a hydrogel to serve as an ideal implant. The viability of NSCs on hydrogels of different components was assessed using calcein-AM/PI staining and the CCK-8 assay for *in vitro* compatibility. No significant differences were noted in cell density among different intervention days for each group (Fig. S2A and B, ESI†). The biocompatibility of hydrogels implanted in the rats was further assessed *in vivo*. First, we performed a blood compatibility evaluation for the hydrogels. After co-incubation with arterial blood, the supernatants extracted from GM, GMP, and GMPT groups appeared pale yellow compared to those from the positive group (Fig. S2D, ESI†). Meantime, the hemolysis ratios in the GMPT group (HR% = 1.18%, Fig. S2D, ESI†) were significantly lower than those in the other hydrogel groups (GM group = 4.88%, GMP group = 2.97%); however, the non-hemolytic standard (hemolysis below 2%) of the American Society for Testing and Materials (ASTM F756–00, 2000) was met. These results showed that the GMPT hydrogel displayed characteristics pertaining to suitable hemocompatibility. Second, the indicators of CRP and ESR were analyzed for implantation of the hydrogels after 28 days post-injury to evaluate the host response. The outcomes of CRP and ESR in the GMPT group were mildly elevated compared to those in the sham group (Fig. S2C–E, ESI†); however, no statistical difference was observed. Next, we assessed the expression of inflammatory factors (NF-κB, TNF-α, and IL-10) at the interface between the spinal cord tissue and the hydrogels. The results of the IHC analysis indicated that the pro-inflammatory factors NF-κB and TNF-α were expressed at low levels in the GMPT group than those in the SCI and sham groups. Conversely, the expression of anti-inflammatory factor IL-10 was higher in the GMPT group than that in the SCI group. This was evident from the data presented in Fig. S3A–D (ESI†). Finally, to investigate whether the GMPT hydrogel was damaging to the visceral organs, we performed HE staining on rat organs. Pathological results showed no significant histological differences in the heart, liver, spleen, lungs, kidneys, and small intestine between rats implanted with the GMPT hydrogel and the sham group (Fig. S3E, ESI†). The above findings indicated that the GMPT hydrogel had good biocompatibility for spinal cord injury repair.

The hydrogels were implanted subcutaneously *in vivo* for monitoring degradation. 56 days after the implantation, the GM hydrogel degraded (Fig. S4C, ESI†) almost entirely. In contrast, the diameter and thickness of the GMP and GMPT hydrogels gradually decreased and retained a few scattered undegraded conductive particles (PPy nanoparticles) (Fig. S4C, ESI†). These results indicated that the degradation rate of GMP and GMPT hydrogels was significantly lower than that of GM hydrogels. Moreover, the HE staining results showed that the thickness of the inflammatory layer tended to decrease over time as the implantation time of hydrogels in GM, GMP, and GMPT groups, and it was not statistically different among the three groups (Fig. S4D–F, ESI†). However, the inflammatory layer was significantly less in the GMPT group than in other hydrogel groups at days 28 and 56 (Table S1, ESI†). This indicated that the conductive hydrogel combined with TMP had better anti-inflammatory effects and properties of slow degradation.

3.3. GMPT hydrogel promotes neurological functional recovery *in vivo*

We used a standardized complete spinal cord transection animal model to evaluate the therapeutic efficacy of hydrogel implantation *in vivo*. Due to its excellent adhesive properties, the GMPT hydrogel demonstrated intimate integration with the spinal cord tissue (Fig. 2B). Furthermore, the HE and Masson pathological staining showed that in the SCI group, tissue dissolution led to the formation of cystic cavities, accompanied by severe fibrosis (evidenced by fibroblasts and collagen deposition) on sides of the transection, with substantial infiltration of inflammatory cells (Fig. S5A and C, ESI†). In the GMP group, the area of cavitation on the injury site was reduced compared to those in the SCI and TMP groups. However, a considerable amount of undegraded PPy nanoparticles encapsulated by fibrous tissues and infiltration of inflammatory cells was observed in the lesions (Fig. S5A, ESI†). In contrast, the GMPT group exhibited sparse PPy nanoparticles, which were surrounded by relatively fewer collagen fibers. The GMPT group showed a tighter integration between implantation and the normal tissue, with aligned surrounding cells (Fig. S5A, C and Fig. 2B, ESI†). Furthermore, a significant statistical difference was observed in the distance between the broken ends on either side of the spinal cord tissue for all the groups ($P < 0.01$). The SCI group exhibited a notably increased distance compared to other groups ($P < 0.05$), whereas the GMPT group demonstrated the shortest average distance among all the groups ($P < 0.05$) (Fig. S5B, ESI†). These findings suggested that GMPT hydrogel implantation prevented further damage to the adjacent interface tissues or cells as well as effectively mitigated scar formation, thereby promoting tissue regeneration and repair.

Variations in pathological alterations with treatment following SCI could lead to differential degrees of neurologic functional recovery. Functional recovery in rats after SCI was assessed using the BBB score and the angle-board test. Prior to the injury, all rats showed a normal range of motor activity in their hindlimbs. After modeling, the rats immediately exhibited complete paralysis of the hindlimbs and gradually regained motor functions by postoperative day 3 (Fig. 2D, E and Tables S2, S3, ESI†). After 28 days of the spinal cord injury,

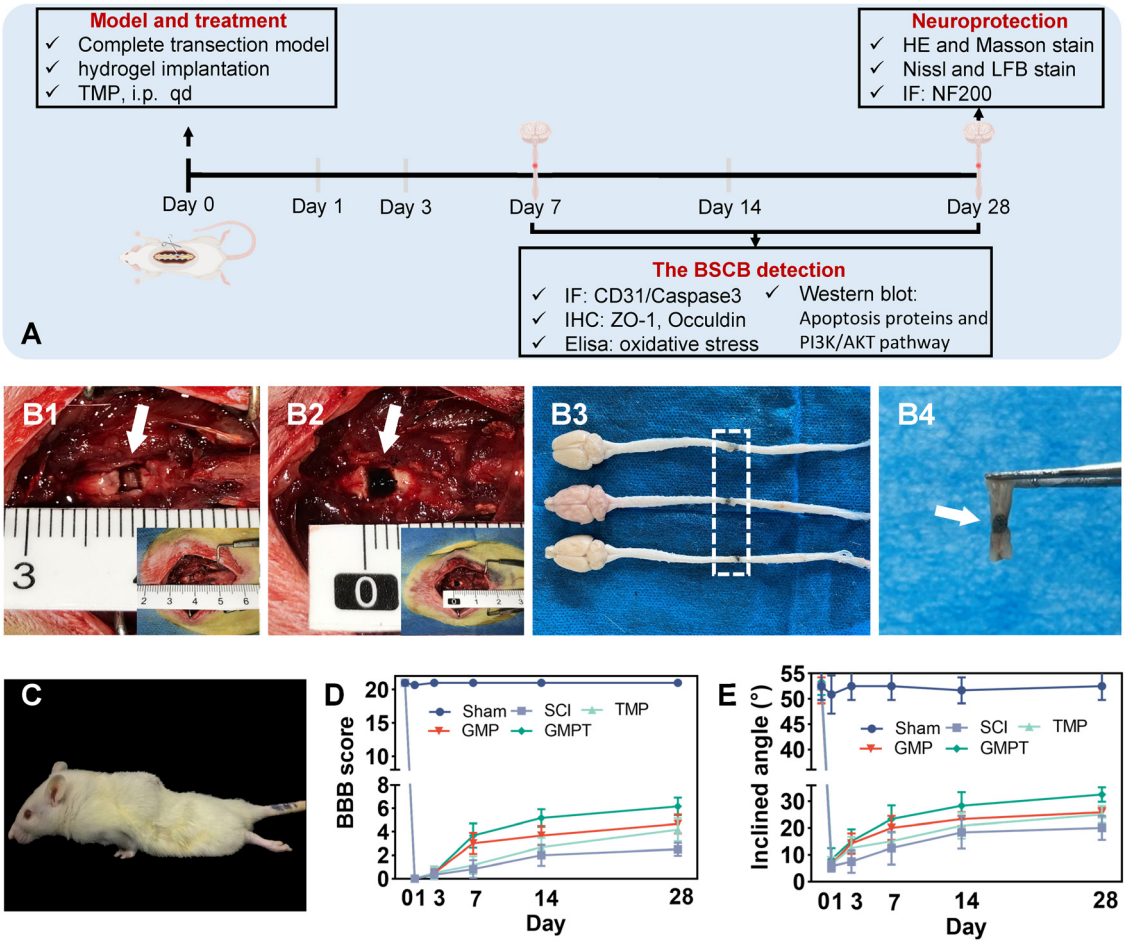

Fig. 2 Hydrogels could promote the repair of spinal cord injuries *in vivo*. (A) Schematic representation of indicator analysis at different time points. After the removal of 2 mm of the complete spinal cord tissue with homemade microscopic double-edged scissors (B1), the GMPT hydrogel was implanted into the gap (B2). When the spinal cord tissue was sampled 28 days after injury, the results showed similar damage areas, suggesting homogeneity of the modeling and GMPT hydrogel implantation segments (B3). (B4) The hydrogel bonded the damaged tissue completely and tightly. (C) After the surgery of complete spinal cord transection, rats awakened from anesthesia showed paralysis of both hind limbs. The BBB score (D) and modified Rivlin-Tator angleboard test (E) were used to assess the hindlimb locomotor function recovery of the model rats (n = 6). Groups were analyzed with a one-way ANOVA and a Bonferroni multiple comparison test.

the SCI group showed the poorest performance concerning BBB scores and hindlimb climbing angles compared to the other intervention groups, indicating limited self-healing capacity in the SCI group. Conversely, both GMP and GMPT groups demonstrated a statistically significant increase in score at postoperative days 7 and 14. However, the GMPT group showed superior improvement in motor function recovery compared to the GMP and TMP groups at 14 days post-operation (Fig. 2D, E and Tables S2, S3, ESI†). Moreover, the GMPT group displayed considerable movements across all three hindlimb joints 28 days post-operation (BBB scoring 7 to 8), whereas the rats in the other treatment groups mainly exhibited extensive activities in two joints and slight movements in one joint of their hindlimbs (BBB scoring 6). The results indicated that electroconductive hydrogels alone promoted neural functional recovery more effectively than intraperitoneal drug injections; however, the combination of both the strategies significantly enhanced functional recovery following SCI.

3.4. GMPT hydrogel acts on neurons to promote survival and repair *in vivo*

To further explore the underlying mechanisms by which the GMPT hydrogel promoted neurological functional recovery after SCI, we utilized histopathological staining to observe axonal remyelination and neuronal survival. Nissl staining results indicated that, in the SCI group, nearly nil neuronal cells were detected. In TMP and GMP groups, only a minimal number of residual neurons were observed around the injury site with an irregular morphology. In contrast, the GMPT group demonstrated neurons that survived and did not undergo massive apoptosis/death in the grey matter on both sides of the lesions (Fig. 3C). Furthermore, the number of Nissl bodies at the caudal regions was compared and found to be the highest in the GMPT group, relatively low in the GMP hydrogel treatment, and much lower in the SCI and TMP groups (Fig. 3D). These findings suggested that the combination of the conductive hydrogel with TMP effectively preserved the survival of neurons

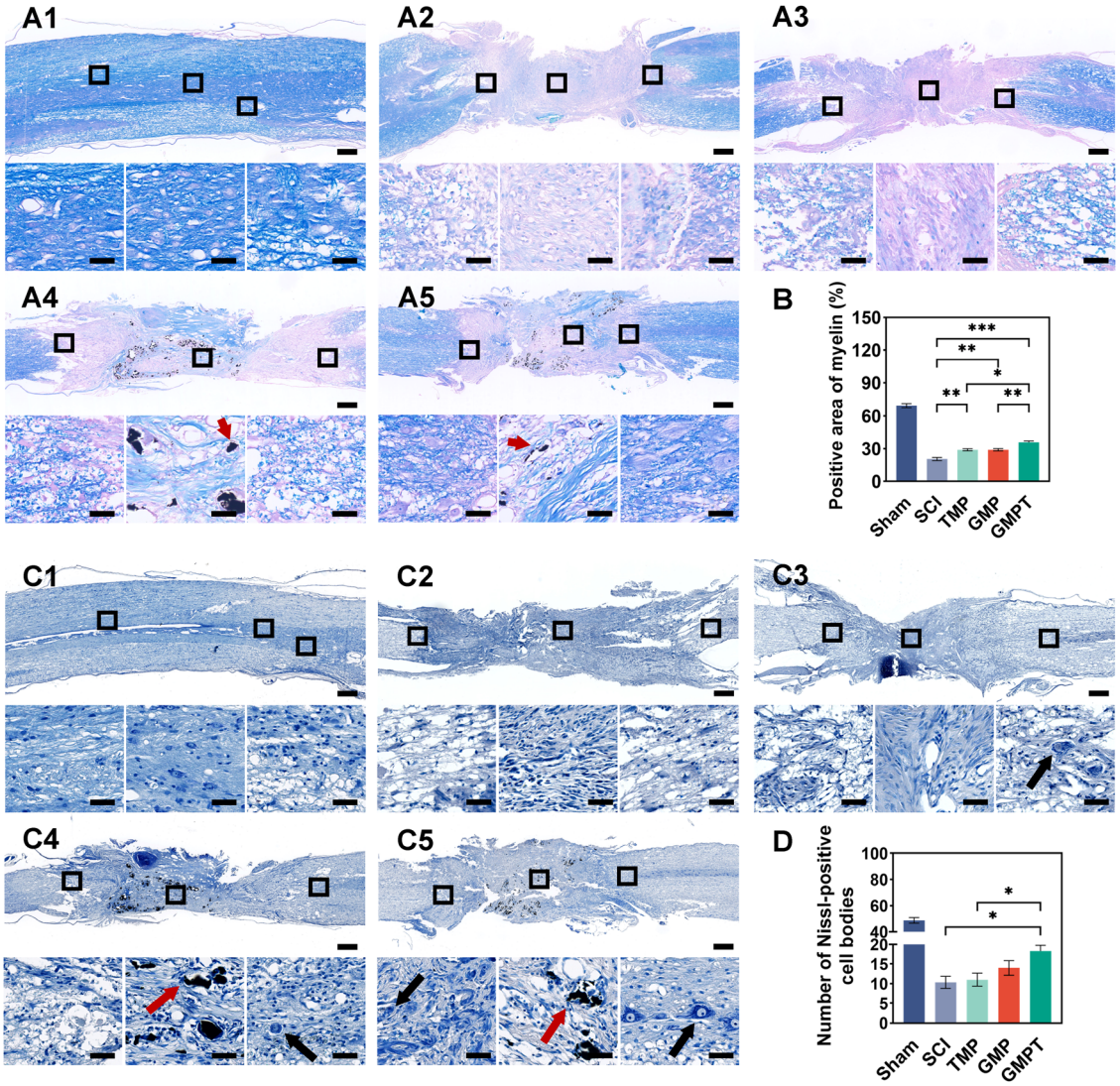

Fig. 3 GMPT hydrogel protected neurons from cell death and decreased axonal injury *in vivo*. LFB staining was used to observe alterations in the myelin sheath morphology for sham (A1), SCI (A2), TMP (A3), GMP (A4), and GMPT groups (A5) 28 days after the injury. The scale bars are 0.6 mm and 40 μm. (B) For different groups, positive myelin staining was expressed as a percentage of the total area measured. (C1–C5) Results of Nissl staining 28 days after SCI in sham, SCI, TMP, GMP, and GMPT groups, respectively. (D) Statistics of the number of Nissl-positive cell bodies in the region adjacent to the caudal end of the injury. Red arrows indicate the conductive particles. Black arrows indicate the remnants of the Nissl bodies. The scale bars are 0.6 mm and 40 μm (n = 6). Groups were analyzed with a one-way ANOVA and a Bonferroni multiple comparison test (*P < 0.05, **P < 0.01, ***P < 0.001).

around the injury site. Moreover, LFB staining further revealed that the GMPT group exhibited relatively compacted myelin structures in the caudal and rostral regions, with a notable positive area of myelin compared to that in the SCI, TMP, and GMP groups (Fig. 3B). Meanwhile, nerve myelin was detected around the PPy nanoparticles at the injury site in the GMPT group, while the density of myelin was significantly higher in the GMP group (Fig. 3A). These results suggested that a combinatorial therapeutic approach could effectively moderate neuronal damage and promote myelinated nerve fiber growth. Furthermore, NF-positive fibers in longitudinal sections of the spinal cord were further analyzed across different groups. The GMPT group displayed the highest overall positive expression, followed by the GMP group, and the TMP and SCI groups demonstrated the lowest expression levels. Additionally, while the density of NF-positive fibers in the injury site of the GMPT group did not show significant statistical differences compared to that in the GMP group (Fig. S6F, ESI†), a pronounced increase in neurofilament intensity was observed in the caudal regions, which surpassed that of the GMP group (Fig. 4F). These neurohistological alterations demonstrated that the GMPT hydrogel had a protective effect on neurons in adjacent interface regions and it also efficiently promoted nerve repair.

3.5. GMPT hydrogel alleviates the disruption of BSCB *in vivo*

Cells that survived around the lesions were crucial for repairing neurovascular damage at the injury site. Furthermore, the maintenance of the structural and functional integrity of the

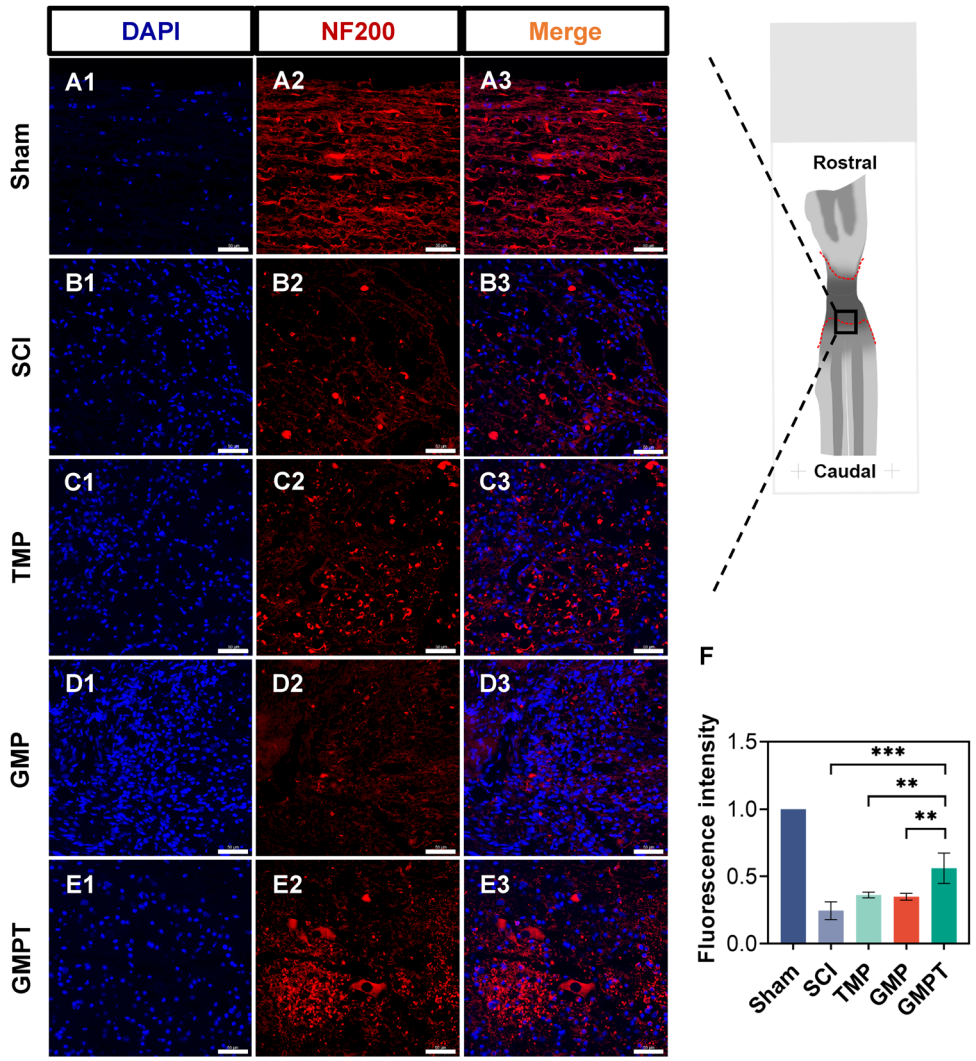

Fig. 4 Neuroprotective effects after SCI were enhanced by GMPT hydrogel implantation. (A)–(E) Alteration of neurofilaments (NFs) in the interface adjacent to the caudal end of the injury is shown here. The NF intensity was quantified from the same area 28 days after injury in different groups (F). The fluorescence intensity of NFs was normalized relative to the sham group for quantification. Red immunofluorescent staining represents the NF-axonal marker. The scale bar is 50 μm (n = 6). Groups were analyzed with a one-way ANOVA and a Bonferroni multiple comparison test (*P < 0.05, **P < 0.01, ***P < 0.001).

BSCB played a vital role in determining cellular viability. We indirectly investigated how the GMPT hydrogel modulated the BSCB to protect neurons in the adjacent regions by examining pathological alterations and expression of related proteins. The tight junction proteins (ZO-1 and occludin) were detected using immunohistochemical staining to evaluate BSCB permeability. Seven days post-injury, the expression level of occludin in the adjacent region was significantly upregulated for the GMPT group compared to the SCI group, while ZO-1 showed no significant difference (Fig. 5C and D). At 28 days postoperatively, occludin and ZO-1 expression was significantly upregulated in the GMPT group, which was higher than that of the other groups (Fig. 5E and F). Moreover, the expression levels of tight junction proteins in all the groups demonstrated a progressive increase from 7 days to 28 days post-intervention (Fig. 5C–F). However, the GMP group had a significantly lower expression level of tight junction proteins than the TMP and GMPT groups (Fig. 5E and F), which indicated that individual treatment strategies for GMP or TMP may not effectively reduce the BSCB permeability. The combined application of both the agents appeared to synergistically mitigate the degradation of those proteins and preserve the integrity of the barrier.

To further investigate the structural integrity of the BSCB, we examined endothelial cell apoptosis around the injury site. 7 days post-injury, apoptotic endothelial cells and some microvascular were visible in the TMP group. The microvascular density was significantly lower in the GMP group than that in the TMP group. Furthermore, it was observed that many apoptotic cells originating from non-endothelial cells were present in the GMP group (Fig. 6C and D). In contrast, the GMPT group showed a significant increase in the expression intensity of $CD31^+$ endothelial cells, with the apoptotic cell

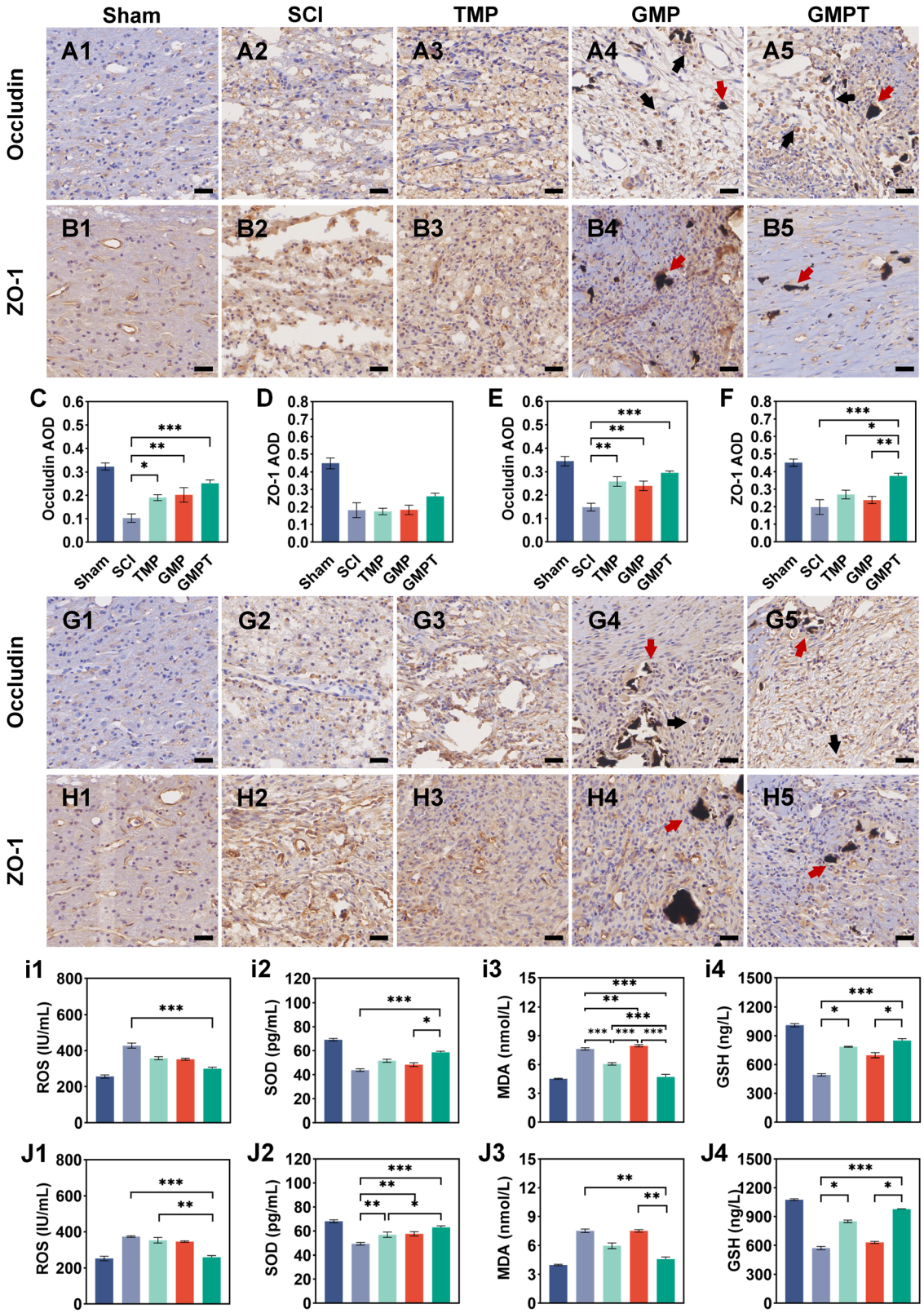

Fig. 5 GMPT hydrogel regulated the blood–spinal cord barrier permeability. IHC was used to evaluate tight junction proteins (ZO-1 and Occludin) adjacent to the injury interface at 7 (A) and (B) and 28 (G) and (H) days after SCI. Red arrows indicate conductive particles. Black arrows indicate the occludin-positive expression. The scale bar is 40 μm. The mean optical density values of ZO-1 and occludin at 7 days (C) and (D) and 28 days (E) and (F) after injury were analyzed semi-quantitatively (n = 6). The expression of oxidative stress indicators in the injury region was measured by the enzyme-linked immunosorbent assay (ELISA) at 7 days (i1)–(i4) and 28 days (J1)–(J4) after SCI (n = 6). Groups were analyzed with a one-way ANOVA and a Bonferroni multiple comparison test (*P < 0.05, **P < 0.01, ***P < 0.001).

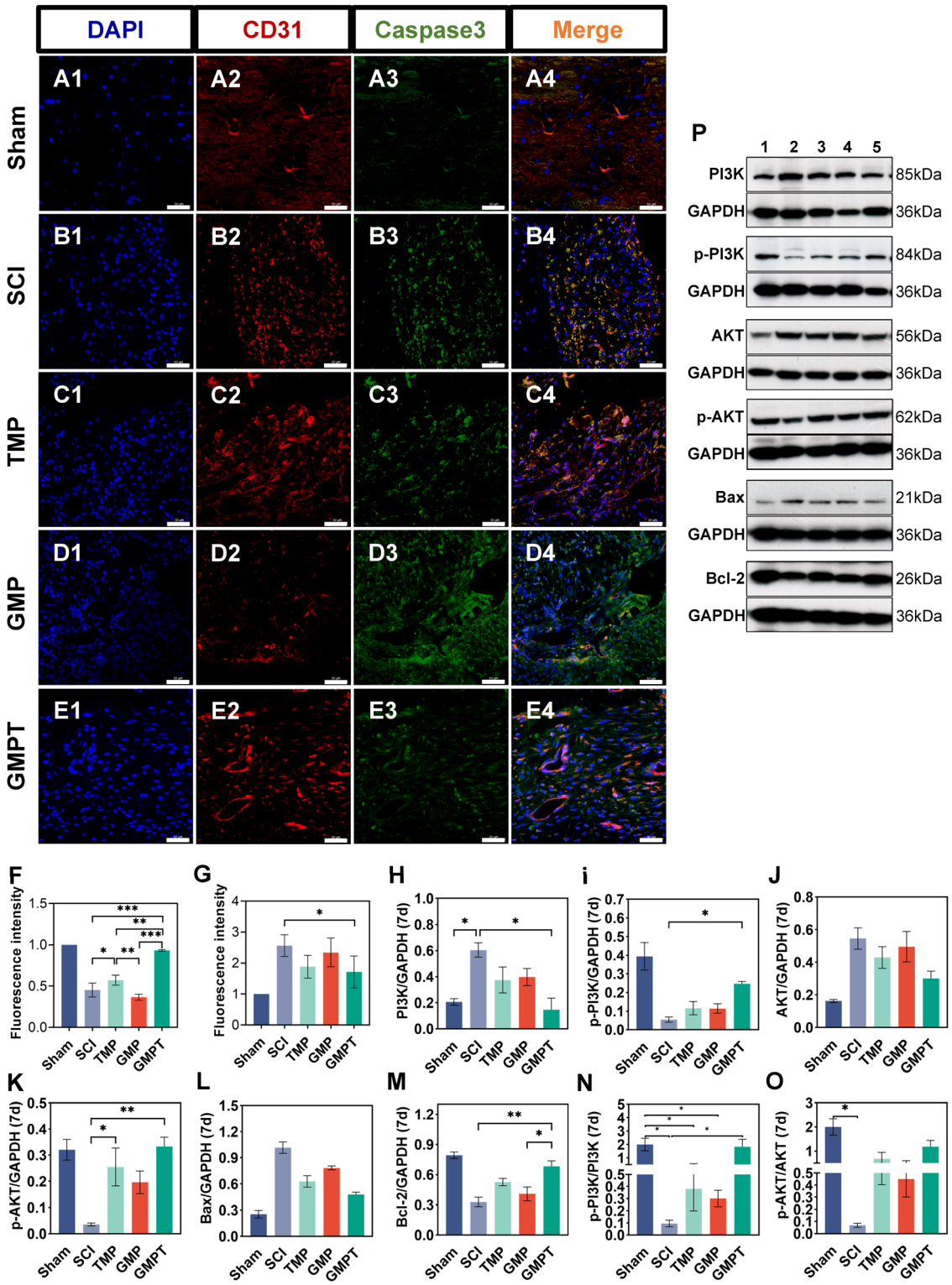

Fig. 6 GMPT hydrogel reduces endothelial cell apoptosis. (A)–(E) Within the peri-lesional area at day 7 after spinal cord injury, apoptosis of endothelial cells was evaluated for different treatment groups using IF imaging. Red IF represented the endothelial cell marker CD31, whereas green IF represented the apoptotic marker caspase3. The scale bar is 50 μm. The fluorescence intensity of CD31 (F) and Caspase3 (G) was normalized relative to the sham group for quantification. The western blot was used to detect the expression of the PI3K/AKT pathway and apoptosis-related proteins for 7 days after SCI. (H)–(M) Protein band intensity (PI3K, p-PI3K, AKT, p-AKT, Bax, and Bcl-2) was quantified (n = 3). Relative protein expression of p-PI3K/PI3K (N) and p-AKT/AKT (O) is demonstrated here. (P) The groups labeled 1 through 5 correspond to sham, SCI, TMP, GMP, and GMPT cohorts, respectively. Groups were analyzed with a one-way ANOVA and a Bonferroni multiple comparison test (*$P < 0.05$, **$P < 0.01$, ***$P < 0.001$).

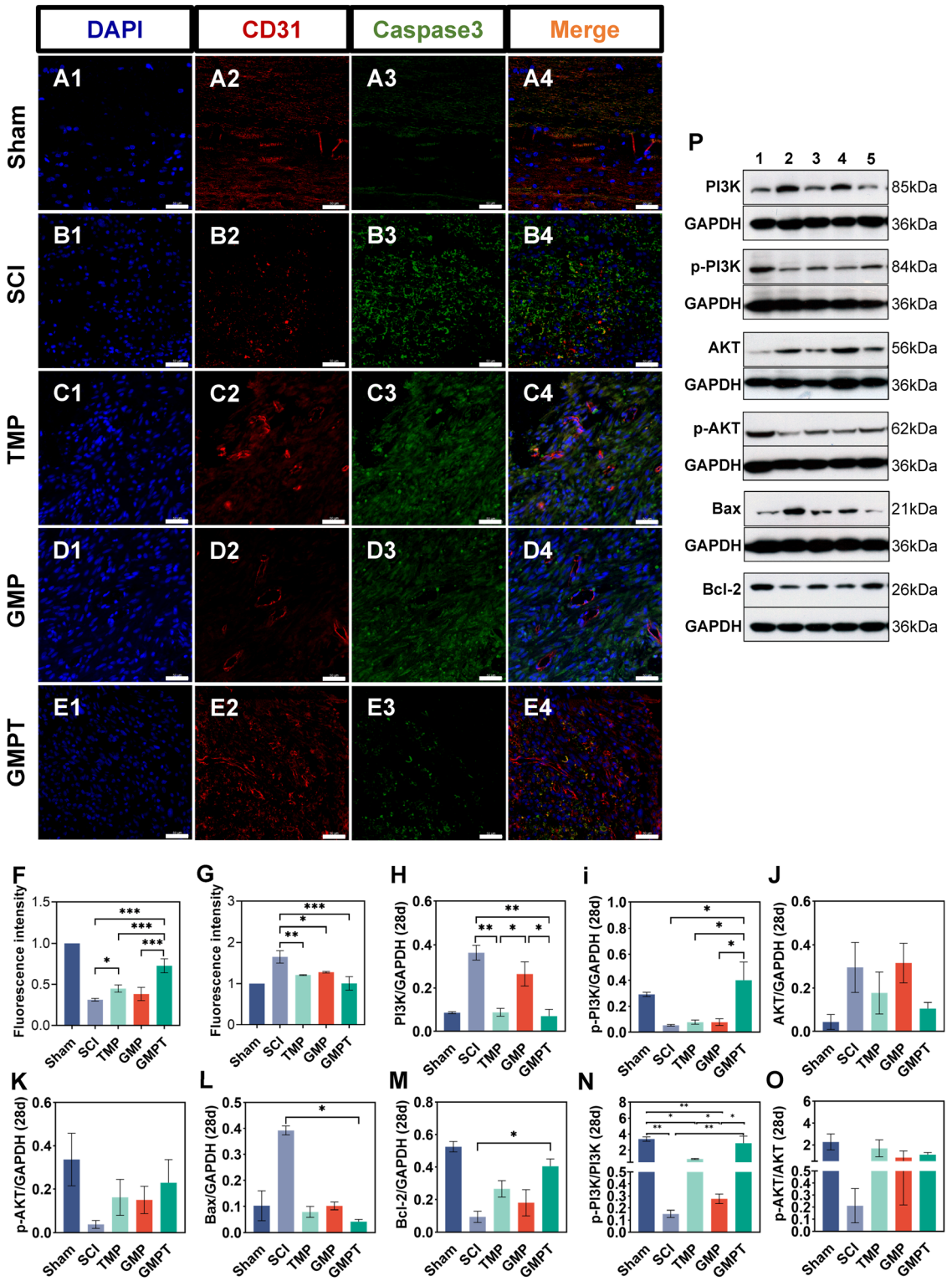

Fig. 7 GMPT hydrogel reduces endothelial cell apoptosis. (A)–(E) At day 28 post-spinal cord injury, endothelial cell apoptosis within the peri-lesional area was evaluated for different treatment groups using IF imaging. Red IF represents the endothelial cell marker CD31, whereas green IF represents the apoptotic marker caspase3. The scale bar is 50 μm. The fluorescence intensity of CD31 (F) and Caspase3 (G) was normalized relative to the sham group for quantification. The western blot was used to detect the expression of the PI3K/AKT pathway and apoptosis-related proteins for 28 days after SCI. (H)–(M) Protein band intensity (PI3K, p-PI3K, AKT, p-AKT, Bax, and Bcl-2) was quantified (n = 3). Relative protein expression of p-PI3K/PI3K (N) and p-AKT/AKT (O) is shown here. (P) The groups labeled 1 through 5 correspond to sham, SCI, TMP, GMP, and GMPT cohorts, respectively. Groups were analyzed with a one-way ANOVA and a Bonferroni multiple comparison test (*$P < 0.05$, **$P < 0.01$, ***$P < 0.001$).

count being notably lower than that in the SCI, TMP, and GMP groups (Fig. 6E–G). At 28 days post-surgery, apoptosis of endothelial cells notably reduced across all the groups compared to that in the prior period. No significant indications of cellular apoptosis were observed in the GMPT group (Fig. 7E). Moreover, the microvascular density was the highest in the GMPT group, relatively low in the GMP hydrogel and TMP-treated groups, and much lower in the SCI group (Fig. 7E and F). These results further suggested that TMP-loaded conductive hydrogels were more advantageous in protecting endothelial cells and maintaining the substructure of the BSCB. Moreover, the western blot results were consistent with the fluorescence analysis. At 7 and 28 days post-injury, the expression levels of the apoptotic protein (caspase3) and pro-apoptotic protein (Bax) were lower in the GMPT group than those in the SCI, TMP, and GMP groups. Conversely, the anti-apoptotic protein (Bcl-2) was higher in the GMPT group than that in the other three groups (Fig. 6G–M and 7G–M).

In addition, the signaling pathways mediating cell apoptosis and oxidative stress biological processes were further investigated by western blotting and ELISA. The ELISA results showed that the endogenous oxidative stress pathways were activated at 7 and 28 days after injury. The GMPT hydrogel group inhibited the expression of oxidative markers (ROS and MDA) at both time points of observation while upregulating the expression of antioxidant indicators SOD and GSH (Fig. 5i and J). Upon comparing the different groups, the GMPT group showed a superior ability to modulate oxidative stress responses, implying that using the combinational method of sustained drug release could be superior to the conventional mode of drug delivery or the application of conductive hydrogels alone. Moreover, the WB analysis suggested that the p-PI3K/PI3K ratio in the GMPT group was significantly higher than that in SCI, TMP, and GMP groups at 7-day and 28-day time points. Meanwhile, the p-AKT/AKT ratio was better than the other three groups at all the time points except for the 28-day p-AKT/AKT ratio, which was better in comparison with the SCI group alone (Fig. 6N, O and 7N, O). This suggests that the GMPT hydrogel may mainly upregulate PI3K/AKT pathways during the acute phase to promote nerve repair.

4. Discussion

After SCI, a cascade of subsequent secondary damage limits the repair and regeneration of nerves.[2,3] When surgical interventions and pharmacological treatments fall short in modulating secondary damage and promoting neural repair, hydrogels loaded with drugs, cells, or growth factors offer a promising novel approach for SCI repair.[2,23] Hydrogels are usually designed based on the physical characteristics of the native tissue and the pathophysiological mechanisms after SCI. Through tissue engineering technologies, such as personalized 3d printing, nucleic acid nanoassemblies, *etc.*, a variety of natural and synthetic materials are accurately manufactured into the required neural repair scaffold.[25,33,34] They bridge the primary spinal cord gap by implantation, injection, or patch methods as well as facilitate in sustaining the slow release of the delivered drugs to address secondary injuries.[23,35,36] The GelMA hydrogel is a quintessential photo-crosslinkable gel that rapidly solidifies under the influence of a photoinitiator. The combination of methacrylate and lysine groups in GM hydrogels confers good mechanical strength and swelling rate, while also providing appropriate sites for cell adhesion. Consequently, cell migration and growth are facilitated.[29,37] Moreover, polymer polypyrrole with high electrical conductivity is added to the GelMA gel as a dopant, and the novel conductive hydrogel effectively enhances the intercellular bioelectrical signal transmission as well as loads the drugs to repair the spinal cord injury.[22]

TMP is a bioactive alkaloid meticulously isolated and purified from the natural herb *Ligusticum chuanxiong* and has remarkable ability to cross the blood–brain/spinal cord barrier. It exhibits a spectrum of pharmacological activities including improvement of microcirculation, attenuation of inflammatory responses, and modulation of neuronal apoptosis.[12,16,17,31] However, the suboptimal bioavailability associated with traditional formulations hinders its potential for effective therapeutic repair.[20,38] Therefore, by exploiting the unique physicochemical properties of the GMP hydrogel, we used a photo-crosslinking approach to load TMP and prepare an electroconductive hydrogel embedded with TMP (GMPT hydrogel). Through *in vitro* dialysis experiments, we confirmed the sustained release of TMP from the GMPT hydrogel. Furthermore, an ideal implant material must simultaneously meet criteria such as mechanical properties, biocompatibility, and biodegradability, which serve as fundamental requirements for its applicability.[39] In this study, combining polypyrrole and TMP increased the cross-linking density within the hydrogel, thereby increasing its average storage modulus. This provided stable mechanical properties to the GMPT hydrogel, which better matched the modulus of elasticity (600–3000 Pa) of the spinal cord tissue, thus providing an optimal mechanical microenvironment for neural cells. The GMPT hydrogel also exhibits commendable electrical conductivity. This ensures the preservation of an electrical microenvironment essential for neural regeneration as well as facilitates damage repair.[40,41] Meantime, the degradability of the hydrogel material should match the nerve regeneration process to provide a stable and suitable regeneration space for the nerve axons. Neural regeneration typically takes place over several months or even years, and the degradation rate of the implant may influence the pathophysiological course of regeneration.[2,35,39] Following implantation, the GMPT hydrogel showed sustained degradation for at least 56 days, facilitating the sustained release of the drug, thereby promoting long-term repair at the injury site. However, the degradation products containing PPy nanoparticles remain controversial due to their slow degradation rate and biosafety concerns.[42] Previous studies have suggested that RAW264.7 macrophages and monocytes are the primary cells responsible for the degradation of PPy.[22] HE staining in this study also showed that at 28 days after implantation of GMP and GMPT hydrogels, PPy surrounded by monocytes was

still present subcutaneously in the rats. By week 8, most of the PPy nanoparticles had degraded. This suggests that PPy has the potential to induce immune-inflammatory responses and may be gradually degraded by endocytosis of monocytes. However, our findings showed that the thickness of the skin's inflammatory layer in the GMPT group was significantly lower than that in the GMP group. This indicates that the combination of TMP can alleviate this effect, thereby reducing the intensity of the inflammatory response and accelerating PPy degradation. Furthermore, the excellent biocompatibility of the hydrogel plays a crucial role in its clinical application. Experiments on cytocompatibility indicated that the GMPT hydrogel lacks evident cytotoxicity. Moreover, experiments on histocompatibility reveal that the GMPT hydrogel is classified as a non-hemolytic material, which follows the requirements for the application of medical biomaterials. The hydrogel could increase the expression of anti-inflammatory factors significantly at the adjacent interface but also ensure that its degradation products do not cause any apparent damage to vital systemic organs.

To investigate the effectiveness of GMPT in promoting neurological recovery after SCI, the hydrogel was implanted into a complete transection of the spinal cord. Behavioral assessments confirmed that the GMPT group displayed a significantly more substantial therapeutic impact regarding improvement in motor deficits in spinal cord injury rats than the SCI, TMP, and GMP groups. Subsequently, we further explored why the GMPT hydrogel promotes the recovery of neurological functions after SCI using histopathological staining. After acute traumatic injury, ischemic necrosis of neurovascular structures and axonal demyelination appeared in the damaged area and surrounding spinal tissues, causing cystic cavities to develop gradually.[2,5,17] In this study, HE pathological staining showed the formation of cavities in the interface of the lesions in all the groups at 28 days post-surgery, with the GMPT group exhibiting the most minor cavity area compared to the other groups. Moreover, the length of the longitudinal axis breaks in the spinal cord tissue in the SCI group was significantly increased compared to that in the control group. This may be due to the gradual dissolution and necrosis of the normal spinal cord tissue around the injury site due to ischemia and hypoxia. In contrast, implantation of the GMPT hydrogel bridged the spinal cord cavities and reduced further harm to the adjacent tissue or cells. The proliferation of the scar tissue is a significant obstacle to the recovery of neural functions, and this scarring differs from the glial scar produced by astrocytes as it is induced by interactions between inflammatory cells and fibroblast-like cells, causing fibrous scarring.[27,43,44] In this study, we analyzed the increase in fibers after spinal cord injury using Masson staining to assess the effect of implanting the GMPT hydrogel on fibrous connective tissues. Our findings imply that implanting the GMPT hydrogel effectively reduced the collagen volume fraction in the injured area while avoiding triggering an excessive inflammatory response and reducing proliferation of the fibrous connective tissue.

Nissl bodies are typical structures of central neurons and are essential sites for protein synthesis within neurons. When neurons undergo damage, alterations occur in the morphology and number of these structures.[2] Evaluating the number and structure of Nissl bodies can offer insights into the functional state of neurons. This study found that the GMPT group presented a significantly higher number of Nissl bodies surrounding the lesions than other intervention groups. The morphology of Nissl bodies also seemed more normalized in the GMPT group, indicating that the GMPT hydrogel had a protective effect on the neurons that might be closely associated with the sustained release of TMP. LFB staining results also indicated that in the GMPT group, neural fibers were arranged in a more orderly manner with compacted myelin structures, and the positive area of myelin was notably larger than that in other intervention groups. This observation aligned with our preliminary findings, which suggested that conductive polymers could promote the restoration of injured spinal cord conduction, thereby inducing axonal regeneration. Simultaneously, the distribution of NF-positive fibers further provided evidence of the efficacy of the GMPT hydrogel in promoting neural repair. The axonal structure significantly reflects the integrity of neuronal structures. Furthermore, NF200, which is a component of neurofilaments, plays a vital role in this function.[2] Our findings indicated that after SCI, the GMPT hydrogel resulted in a superior expression of NF neural fibers both in the injury core and its periphery to that in the TMP and GMP groups. This implies that using the combinational method of sustained drug release could be superior to the conventional mode of drug delivery or the application of conductive hydrogels alone. Furthermore, these pathological results suggested that the conductive hydrogel loaded with TMP exerted neuroprotective effects on the adjacent regions and possessed therapeutic potential in promoting axonal regeneration.

BSCB integrity is a crucial factor for neural repair. The barrier relies significantly on the structural and functional integrity of endothelial cells as a substructure.[3] Preventing the apoptosis of these endothelial cells following SCI is essential to maintain the structural integrity of the barrier, which is vital for promoting the survival of the neurons.[3,5,8,9] We evaluated apoptosis in endothelial cells at 7 and 28 days after injury. Our results showed different levels of cell apoptosis in the TMP and GMP groups. Nevertheless, the GMPT hydrogel proved more efficient than the other two groups in preventing endothelial cell apoptosis around the lesions. This suppression effect was markedly present at 7 days after injury. Apoptosis is primarily mediated by endogenous pathways that directly disturb the balance between pro- and anti-apoptotic proteins within the cell. This disturbance causes the activation of caspase3 and caspase9, along with the release of mitochondrial cytochrome *C*.[45,46] Consequently, the ratio of the apoptosis inhibitor protein (Bcl-2) to the pro-apoptosis protein (Bax) is pivotal in determining cell survival or apoptosis. In this study, we observed that the expression of pro-apoptotic proteins (Bax and caspase3) was significantly upregulated at various time points after SCI, whereas the expression of anti-apoptotic protein (Bcl-2) decreased. GMPT hydrogels increased the Bcl-2 expression considerably at all time points after the

intervention. However, their inhibitory effects on pro-apoptotic proteins were less pronounced. Thus, we speculated that the GMPT hydrogel inhibits endothelial cell apoptosis mainly by upregulating the expression level of Bcl-2. As previously mentioned, the mitochondria-mediated endogenous pathway plays a pivotal role in activating apoptosis. Post-spinal cord injury, local ischemic and hypoxic conditions can lead to mitochondrial dysfunction, resulting in an imbalance between the oxidative and antioxidative systems. This triggers lipid peroxidation reactions, exacerbating cell apoptosis.[45,47,48] Therefore, modulating oxidative stress responses may be a productive strategy to inhibit endothelial cell apoptosis.[14,18,49] We examined the alterations in oxidative stress-related markers at the injury site and the outcomes indicated that endogenous oxidative stress was triggered along with the downregulation of antioxidative proteins (SOD and GSH) and significant upregulation of oxidative proteins (ROS and MDA). However, the GMPT hydrogel effectively alleviated oxidative protein expression while promoting antioxidative proteins' expression level. This observation was consistent with the results of pathological staining of apoptosis in endothelial cells. These outcomes suggested that the GMPT hydrogel might modulate oxidative stress-inducing apoptosis for promoting endothelial cell survival.

Furthermore, the PI3K/AKT pathway is a pivotal signaling pathway that is intimately associated with the pathological process of SCI. Activation of this pathway can promote neural functional recovery post-spinal cord injury by modulating various biological processes.[2,22] Pertinent studies have indicated that the PI3K/AKT pathway can regulate the expression of mitochondrial membrane permeability proteins Bcl-2 and Bax, exerting anti-apoptotic effects.[9] This research found that the ratio of phosphorylated to non-phosphorylated proteins (p-PI3K/PI3K and p-AKT/AKT) was up-regulated during both the assessed periods after GMPT hydrogel intervention compared to that in the SCI groups, with statistically different outcomes. This implied that the primary target of action for the GMPT hydrogel might be the PI3K pathways. Moreover, we observed a positive correlation between the expression levels of p-PI3K and Bcl-2, while a negative correlation was noted with Bax and caspase-3, which was consistent with previous research findings. Nevertheless, no rescue experiments were conducted in this study. Thus, drawing upon the extant literature,[12,50] we postulated that the GMPT hydrogel may modulate endothelial cell apoptosis by regulating the PI3K/AKT axis, thereby preserving the integrity of the barrier. In addition, the destruction of the BSCB is not solely attributable to apoptosis in endothelial cells, but also to the loss of tight junction proteins, which are present between endothelial cells to maintain intercellular spaces and regulate cellular polarity. They restrict the abnormal entry of immune cells and cytokines through the barrier to mitigate secondary injuries.[3] Following SCI, the expression levels of tight junction proteins (ZO-1 and Occludin) were markedly downregulated. Intervention with the GMPT hydrogel significantly upregulated the expression of occludin on day 7 post-injury. By the 28th day post-injury, the expression levels of both the proteins in the GMPT group exhibited an upward trend, notably surpassing those in the TMP and GMP groups. This might be associated with the sustained release of TMP from the GMPT hydrogel, suggesting that the combined application of TMP and GMP hydrogels can synergistically mitigate the degradation of tight junction proteins to reduce the permeability of the BSCB.

However, this study has its limitations. First, the pathological mechanism of spinal cord injury is complex, involving cellular crosstalk and multiple biological pathways. This study solely focused on changes in the blood–spinal barrier and its substructures *in vivo*, as well as the regulation signal of the PI3K and oxidative stress-related pathways. Moreover, the evaluation was limited to the subacute stage and did not include the chronic stage. Finally, the impact of hydrogel's conductive properties on cells has not been extensively researched. Using external electrical stimulation or analysis of cell electrophysiological changes by the patch clamp technology or multiple electron arrays might further reveal the underlying mechanism of conductive materials in inducing cell differentiation and axon growth. This will be the focus of our future research.

5. Conclusions

In summary, we constructed a composite conductive hydrogel with the sustained release of a novel drug by loading TMP based on GelMA-PPy as the foundation. This hydrogel displayed excellent physicochemical properties, biocompatibility, and sustained release of the drug. These prominent features alleviate damage to the BSCB, promoting the survival of adjacent neurons and enhancing myelinated axon growth. Furthermore, *in vivo* experiments demonstrated that the GMPT hydrogel is more favorable for treating spinal cord injuries than implantation of the GMP hydrogel alone or intraperitoneal injection of TMP. It may exert its effects by synergistically inhibiting the oxidative stress pathway, regulating endothelial cell apoptosis *via* the PI3K/AKT signaling pathway, and mitigating the degradation of junction proteins, thereby protecting BSCB integrity to promote neural functional recovery post-injury. Our study indicates that combining the conductive hydrogel with TMP presents a promising therapeutic strategy for spinal cord injuries.

Author contributions

B. W. D. and G. L. had taken an active part in designing the experiments, jointly implementing animal experiments, and checking the manuscript. S. Y. S. and X. Y. L. analysed the data. Y. Z. and J. P. R. made professional figures and language polishing. C. Y. N., L. H. L., and X. H. M. evaluated the data and amended the manuscript.

Conflicts of interest

The authors declare that there are no existing conflicts of interest.

Acknowledgements

This work was supported partly by the grant from the National Natural Science Foundation of China (Grant No. 82305271). In addition, some illustrations in article were created by BioRender.com.

References

1 B. Zheng and M. H. Tuszynski, *Nat. Rev. Mol. Cell Biol.*, 2023, **24**, 396–413.
2 X. Hu, W. Xu, Y. Ren, Z. Wang, X. He, R. Huang, B. Ma, J. Zhao, R. Zhu and L. Cheng, *Signal Transduction Targeted Ther.*, 2023, **8**, 245.
3 L. Y. Jin, J. Li, K. F. Wang, W. W. Xia, Z. Q. Zhu, C. R. Wang, X. F. Li and H. Y. Liu, *J. Neurotrauma*, 2021, **38**, 1203–1224.
4 R. Zhou, J. Li, Z. Chen, R. Wang, Y. Shen, R. Zhang, F. Zhou and Y. Zhang, *J. Neuroinflammation*, 2023, **20**, 118.
5 C. Dray, G. Rougon and F. Debarbieux, *Proc. Natl. Acad. Sci. U. S. A.*, 2009, **106**, 9459–9464.
6 Z. You, X. Gao, X. Kang, W. Yang, T. Xiong, Y. Li, F. Wei, Y. Zhuang, T. Zhang, Y. Sun, H. Shen and J. Dai, *Bioact. Mater.*, 2023, **29**, 36–49.
7 W. Xin, Z. Baokun, C. Zhiheng, S. Qiang, Y. Erzhu, X. Jianguang and L. Xiaofeng, *Acta Biomater.*, 2023, **159**, 140–155.
8 Z. He, J. Du, Y. Zhang, Y. Xu, Q. Huang, Q. Zhou, M. Wu, Y. Li, X. Zhang, H. Zhang, Y. Cai, K. Ye, X. Wang, Y. Zhang, Q. Han and J. Xiao, *Theranostics*, 2023, **13**, 849–866.
9 R. Zhao, X. Wu, X.-Y. Bi, H. Yang and Q. Zhang, *Neural Regener. Res.*, 2022, **17**, 1080–1087.
10 L. Deng, J. Q. Lv and L. Sun, *Front. Pharmacol.*, 2022, **13**, 950368.
11 D. Koushki, S. Latifi, A. Norouzi Javidan and M. Matin, *J. Spinal Cord Med.*, 2015, **38**, 13–22.
12 Y. Liu, G. Yang, W. Cui, Y. Zhang and X. Liang, *Front. Pharmacol.*, 2022, **13**, 948600.
13 H. Shao, X. He, L. Zhang, S. Du, X. Yi, X. Cui, X. Liu, S. Huang and R. Tong, *Front. Pharmacol.*, 2021, **12**, 761722.
14 P. Gong, Z. Zhang, Y. Zou, Q. Tian, S. Han, Z. Xu, J. Liao, L. Gao, Q. Chen and M. Li, *Eur. J. Pharmacol.*, 2019, **854**, 289–297.
15 L. Zhang, X. Lu, L. Gong, L. Cui, H. Zhang, W. Zhao, P. Jiang, G. Hou and Y. Hou, *Cell. Mol. Neurobiol.*, 2021, **41**, 717–731.
16 Y. Fan and Y. Wu, *Biomed. Pharmacother.*, 2017, **94**, 827–833.
17 J. Hu, Y. Cao, T. Wu, D. Li and H. Lu, *Spine*, 2016, **41**, 1272–1278.
18 J. Z. Hu, X. K. Wang, Y. Cao, D. Z. Li, T. D. Wu, T. Zhang, D. Q. Xu and H. B. Lu, *Curr. Neurovasc. Res.*, 2017, **14**, 110–116.
19 Y. Zhang, C. Ma, L. He, L. Liao, C. Guo, C. Wang, L. Gong, H. Zhou, K. Fu, C. Peng and Y. Li, *Oxid. Med. Cell. Longevity*, 2022, **2022**, 2232365.
20 H. Xia, Z. Cheng, Y. Cheng and Y. Xu, *Mater. Sci. Eng., C*, 2016, **69**, 1010–1017.
21 C. Fan, W. Yang, L. Zhang, H. Cai, Y. Zhuang, Y. Chen, Y. Zhao and J. Dai, *Biomaterials*, 2022, **288**, 121689.
22 L. Fan, C. Liu, X. Chen, L. Zheng, Y. Zou, H. Wen, P. Guan, F. Lu, Y. Luo, G. Tan, P. Yu, D. Chen, C. Deng, Y. Sun, L. Zhou and C. Ning, *Adv. Sci.*, 2022, **9**, e2105586.
23 E. A. Kiyotake, M. D. Martin and M. S. Detamore, *Acta Biomater.*, 2022, **139**, 43–64.
24 B. Yang, C. Liang, D. Chen, F. Cheng, Y. Zhang, S. Wang, J. Shu, X. Huang, J. Wang, K. Xia, L. Ying, K. Shi, C. Wang, X. Wang, F. Li, Q. Zhao and Q. Chen, *Bioact. Mater.*, 2021, **15**, 103–119.
25 Q. Zhang, B. Shi, J. Ding, L. Yan, J. P. Thawani, C. Fu and X. Chen, *Acta Biomater.*, 2019, **88**, 57–77.
26 L. Zhou, L. Fan, X. Yi, Z. Zhou, C. Liu, R. Fu, C. Dai, Z. Wang, X. Chen, P. Yu, D. Chen, G. Tan, Q. Wang and C. Ning, *ACS Nano*, 2018, **12**, 10957–10967.
27 Y. Luo, L. Fan, C. Liu, H. Wen, S. Wang, P. Guan, D. Chen, C. Ning, L. Zhou and G. Tan, *Bioact. Mater.*, 2022, **7**, 98–111.
28 W. Liu, Y. Q. Luo, N. Cong, W. G. Zhang, Q. Z. Zhang, H. Zou and C. F. Fu, *J. Nanobiotechnol.*, 2021, **19**, 286.
29 L. Fan, C. Liu, X. Chen, Y. Zou, Z. Zhou, C. Lin, G. Tan, L. Zhou, C. Ning and Q. Wang, *ACS Appl. Mater. Interfaces*, 2018, **10**, 17742–17755.
30 Y. Lin, Y. Wan, X. Du, J. Li, J. Wei, T. Li, C. Li, Z. Liu, M. Zhou and Z. Zhong, *J. Nanobiotechnol.*, 2021, **19**, 28.
31 Z. Jin, J. Liang and P. E. Kolattukudy, *Front. Pharmacol.*, 2021, **12**, 710358.
32 A. S. Rivlin and C. H. Tator, *J. Neurosurg*, 1977, **47**, 577–581.
33 K. Liu, L. S. Yang, R. T. Li, Z. M. Song, J. X. Ding, B. Liu and X. S. Chen, *Adv. Sci.*, 2022, **9**, e2103875.
34 M. N. Zhao, R. J. Wang, K. M. Yang, Y. H. Jiang, Y. C. Peng, Y. K. Li, Z. Zhang, J. X. Ding and S. J. Shi, *Acta Pharm. Sin. B*, 2023, **13**, 916–941.
35 Y. Wang, H. Q. Lv, X. Chao, W. X. Xu, Y. Liu, G. X. Ling and P. Zhang, *Mil. Med. Res.*, 2022, **9**, 16.
36 B. Zhu, G. J. Gu, J. Ren, X. M. Song, J. J. Li, C. Y. Wang, W. C. Zhang, Y. Q. Huo, H. F. Wang, L. Jin, S. Feng and Z. J. Wei, *ACS Nano*, 2023, **17**, 22928–22943.
37 J. W. Nichol, S. T. Koshy, H. Bae, C. M. Hwang, S. Yamanlar and A. Khademhosseini, *Biomaterials*, 2010, **31**, 5536–5544.
38 J. Lin, Q. Wang, S. Zhou, S. Xu and K. Yao, *Biomed. Pharmacother.*, 2022, **150**, 113005.
39 P. Hassanzadeh, F. Atyabi and R. Dinarvand, *J. Controlled Release*, 2018, **279**, 181–197.
40 A. Burnstine-Townley, Y. Eshel and N. Amdursky, *Adv. Funct. Mater.*, 2020, **30**, 1901369.
41 M. Levin, *BioEssays*, 2012, **34**, 205–217.
42 R. Balint, N. J. Cassidy and S. H. Cartmell, *Acta Biomater.*, 2014, **10**, 2341–2353.
43 J. Ruschel, F. Hellal, K. C. Flynn, S. Dupraz, D. A. Elliot, A. Tedeschi, M. Bates, C. Sliwinski, G. Brook, K. Dobrint, M. Peitz, O. Brüstle, M. D. Norenberg, A. Blesch, N. Weidner, M. B. Bunge, J. L. Bixby and F. Bradke, *Science*, 2015, **348**, 347–352.

44 X. Sun, H. Liu, Z. Tan, Y. Hou, M. Pang, S. Chen, L. Xiao, Q. Yuan, B. Liu, L. Rong and L. He, *Small*, 2023, **19**, e2205012.
45 J. L. Wang, X. Luo and L. Liu, *Aging*, 2019, **11**, 12213–12235.
46 T. Y. Yune, J. Y. Lee, M. H. Jiang, D. W. Kim, S. Y. Choi and T. H. Oh, *Free Radical Biol. Med.*, 2008, **45**, 1190–1200.
47 S. Rao, Y. Lin, R. Lin, J. Liu, H. Wang, W. Hu, B. Chen and T. Chen, *J. Nanobiotechnol.*, 2022, **20**, 278.
48 Y. Liang, J. H. Wu, J. H. Zhu and H. Yang, *J. Neurotrauma*, 2022, **39**, 701–714.
49 Y. Wang, T. Wu and M. Tang, *J. Hazard. Mater.*, 2020, **394**, 122439.
50 X. F. Feng, M. C. Li, Z. Y. Lin, M. Z. Li, Y. Lu, Y. M. Zhuang, J. F. Lei, L. Wang and H. Zhao, *Front. Cell. Neurosci.*, 2023, **17**, 1125412.